ELSEVIER

Contents lists available at ScienceDirect

# Chemical Engineering Journal

journal homepage: www.elsevier.com/locate/cej





# The implications of pulsating anode potential on the electrochemical recovery of phosphate as magnesium ammonium phosphate hexahydrate (struvite)

Ruhi Sultana a,b, Lauren F. Greenlee a,b,\*

- a Ralph E. Martin Department of Chemical Engineering, University of Arkansas, 3202 Bell Engineering Center, Fayetteville, AR 72701, United States
- <sup>b</sup> Department of Chemical Engineering, Pennsylvania State University, University Park, PA 16802, United States

# ABSTRACT

A sustainable approach to address the limited availability of rock phosphate is to electrochemically recover phosphorus (P) as struvite (magnesium ammonium phosphate hexahydrate,  $MgNH_4PO_4$ - $6H_2O$ ) fertilizer. On Mg surfaces, however, magnesium hydroxide ( $Mg(OH)_2$ ) and/or struvite form resistive films that limit the release of divalent Mg ions and reduce struvite precipitation. The present work enhances struvite recovery through the application of a dynamic voltage with a sinusoidal waveform. Compared to a constant potential, our results demonstrated that a dynamic potential could enhance the rupture of the passivating film, and facilitate the release of  $Mg^{2+}$  from the metal anode, thereby overcoming passivation problems. Ammonium dihydrogen phosphate ( $NH_4H_2PO_4$ ,  $NH_4PO_4$ ) mM) solutions at neutral pH were used as test solutions. A  $NH_4PO_4$  increase in magnesium release was observed versus constant voltage applications, resulting in a  $NH_4PO_4$  increase in phosphate recovery. The scanning electron microscopy (SEM) and  $NH_4PO_4$  diffraction (XRD) characterizations indicated that the precipitate recovered contained struvite. An analysis of electrode surfaces using laser ablation inductively coupled plasma mass spectrometry (LA-ICP-MS) confirms a greater extent of passivating film breakdown under dynamic voltages.

# 1. Introduction

The unprecedented explosion of the global population has exacerbated a multitude of problems, including food and water shortages. Using phosphate rock mined from the ground as a component of fertilizer, farms are able to grow more crops and feed more than 7 billion people [1,2]. In contrast, excessive application of fertilizers has resulted in the loss of large amounts of nutrients as runoff [3,4]. A surplus of nutrients, such as phosphorus and nitrogen, in wastewater leads to eutrophication of the receiving water bodies and degrades water quality. Phosphorus removal costs are high for both industries and municipalities when attempting to comply with current nutrient discharge conditions [2,5]. For example, the permissible limit of phosphorus in treated municipal wastewater is 0.1 mg L<sup>-1</sup> under the Water Framework Directive of the European Union [6]. As a natural resource, phosphate is limited, and some estimates suggest that the supply of phosphate might be exhausted within the next century [7,8]. Thus, it is crucial to recycle phosphate into a value-added product, such as a renewable fertilizer, through the application of novel and efficient technologies. One such attractive and promising option is to precipitate struvite, a phosphate mineral, by adding water soluble magnesium salts to wastewater

containing nitrogen and phosphorus [9–12]. The corresponding reaction for precipitation of struvite may be expressed according to Eq. (1), where n may vary from 0 to 2 depending upon the pH of the solution [12,13].

$$Mg^{2+} + NH_4^+ + H_nPO_4^{n-3} + 6H_2O \rightarrow MgNH_4PO_4.6H_2O + nH^+$$
 (1)

Struvite is slightly soluble in water, a non-odorous, slow nutrient (Mg, N, and P) releasing mineral, and may be regarded as a premium grade fertilizer [14,15]. To date, chemical precipitation using stirred tank or fluidized bed reactor is most commonly used for struvite production [16]. This method has been further upgraded by augmenting with downstream ion exchange and membrane separation units. In chemical precipitation, various Mg salts and bases are added to water to supply Mg and adjust the pH of the solution [17]. However, the salts (commonly MgCl<sub>2</sub> and MgSO<sub>4</sub>) are to be dosed in excess of the stoichiometric ratio to compensate for the imperfect mixing of NH $_4^+$  and PO $_4^{3-}$  with Mg $^{2+}$ . The use of Mg salts in stoichiometric excess necessarily increases the operating cost of the process. Moreover, low cost salts like MgO and MgCO $_3$  are relatively less soluble in water compared to MgCl $_2$  and MgSO $_4$  [18,19]. Thus, salt replacement may not to lead to any

E-mail address: greenlee@psu.edu (L.F. Greenlee).

<sup>\*</sup> Corresponding author at: Ralph E. Martin Department of Chemical Engineering, University of Arkansas, 3202 Bell Engineering Center, Fayetteville, AR 72701, United States.

tangible economic benefit. On the other hand, electrochemical precipitation of struvite using sacrificial Mg anode is devoid of any salt addition. The release of Mg<sup>2+</sup> through electrode corrosion can also be controlled by tuning the applied potential. Some other advantages of the electrochemical system are automation compatibility, minimal or no chemical addition.and more than 80-90 % nitrogen and 90 % phosphorus removal as precipitates through several reaction mechanisms [16,20–22]. Further cost savings can be achieved by controlling the pH at  $\sim$ 9 to prevent volatilization of NH $_4^+$  to NH $_3$  and also to precipitate high purity struvite. Imperatively, the pH close to anode is higher than the bulk pH because of local alkalization that eventually leads to struvite precipitation even at neutral bulk pH [23]. A novel electrolysis technique developed by Lin et al. successfully removed 93 % of phosphate from biogas digestion slurry at a stable pH of 8.6 without the need for chemical reagents [24]. In a more recent study, Sultana et al. were able to recover ~95 % of phosphate from synthetic wastewater with Cl<sup>-</sup> as background ions at pH 8 [25]. In a pilot plant operated by Fraunhofer Institute for Interfacial Technology and Biotechnology in Germany, P concentrations in domestic wastewater were reduced to 2 mg.L<sup>-1</sup> by 99.7 % using electrochemical struvite technology while using less than 70 Wh.m<sup>-3</sup> energy [26]. Anodic dissolution of Mg<sup>2+</sup> in solution is described as a heterogeneous electron transfer mechanism combined with or followed by a homogeneous chemical reaction (EC) [27]. Upon connecting the Mg anode to a suitable cathodic material (steel, Al, or Zn), galvanic corrosion occurs through the following electrochemical reactions at the electrodes (Eqs. (2), (3), (4)) [28-30].

Reaction at the anode:

$$Mg \rightarrow Mg^+ + e^- \tag{2}$$

$$Mg^{+} + H_{2}O \rightarrow Mg^{2+} + OH^{-} + \frac{1}{2}H_{2}$$
 (3)

Reaction at the cathode:

$$O_2 + 2H_2O + 4e^- \rightarrow 4OH^-$$
 (4)

$$H_2O + 2e^- \rightarrow \frac{1}{2}H_2 + 2OH^-$$
 (5)

Hydrogen generation from anode during magnesium corrosion reaction occurring concurrently with the electrochemical struvite reaction, as well as cathodic hydrogen generation has significant implications for the energy industry, serving as a clean, carbon-free source of energy in a hydrogen economy. According to the U.S. Department of Energy, the levelized cost of hydrogen production will be 1-1.5 \$/kg by 2050, underscoring the importance of cost-effective hydrogen generation processes [31]. Thus, it is possible to offset the costs associated with electrochemical struvite production by profiting from hydrogen by co-generating both struvite and hydrogen. Despite these advantages, electrochemical struvite precipitation technology suffers from electrode passivation that hinders the easy release of Mg<sup>2</sup> particularly at at low voltage conditions. Production of OH- (Eq. (3)) during anodic corrosion raises the pH and forms a layer of Mg(OH)2 on the electrode, providing a barrier against corrosion, commonly referred as "electrode passivation" [25,32,33]. In a recent study by Cai et al., Mg has been reported to oxidize to Mg(OH)<sub>2</sub> (at pH > 10), struvite, and MgCO<sub>3</sub> during electrolysis of solutions containing ammonium and phosphate concentrations [34]. The electrode passivation is considered as the fundamental nonideality of electrochemical struvite precipitation. Several remedial methods were introduced over the last decade to overcome such problem. The effects of ultrasound, chelating agents (e. g., EDTA), and enhanced feedstock salinity were investigated by several research groups to minimize the degree of electrode surface passivation but have resulted in higher solution temperature and altered chemical makeup of the wastewater matrix that naturally the overall cost of struvite recovery [25,35,36]. Hence, a question may be raised about whether electrode fouling (passivation) could be addressed by

modifying or altering the physical variables of the system, which primarily includes electric field variables. The goal of the present study was thus to look for alternative methods of increasing Mg release and subsequently, enhancing the struvite production at low energy budget.

Pulsating electric potential has been demonstrated to efficiently remove heavy metal (i.e., Cr(VI)) in Fe electrocoagulation relative to the constant potential application with identical mean value [37–39]. Current research has shown 'pulse electrolysis' to be a promising alternative to its equivalent potentiostatic applications [40]. With the growing hydrogen economy, there has been a surge in research devoted to enhancing the efficiency of pulsed water electrolysis [41–44]. For example, Vincent et al. investigated hydrogen production on a 3D  $MnO_2$  electrode and recorded the optimal electrolysis condition for a pulse frequency of 500 Hz [45]. Pulsed electrolysis has been widely explored in several electrochemical systems [46–49]. For instance, in an application of electrocatalysis for the oxidation of formic acid, Adzic et al. analyzed the effect of frequency and anodic potential on electrocatalytic activity and observed higher catalytic current at an optimal frequency of 2000 Hz [50].

Drawing inspiration from a multitude of research focused on the applications of pulsation in electrochemical systems, we hypothesized that a pulsating anode potential with an appropriate frequency must induce an optimized cyclic Maxwell stress on the passivation layer and rupture the layer at a relatively lower mean potential than the equivalent constant potential application. Our apprehension is essentially derived from the much explored "fatigue failure" of structural elements at an ultimate stress that is always lower than the respective constant stress experiments. Thus, we have outlined the objective of this study so as to demonstrate the efficacy of pulsating anode potential, in maximizing the production of struvite following the electrochemical precipitation technique using sacrificial Mg electrode. The study also includes a comparative analysis between pulsating and constant potential electrolysis in terms of phosphate recovery, precipitate yield, and morphology. The mean potential, as identified from linear sweep voltammetry analysis was held at the pitting potential at which the struvite yield may be expected to be marginally low. The effect of frequency was investigated over a range of 0.1-100 Hz with synthetic wastewater feedstock containing chloride and sulfate ions as background ions. Synthetic wastewater was specifically chosen to limit the number of the process parameters in this first-of-its-kind analysis. Our findings show an increase in struvite precipitate and a reduction in energy budget in pulsating voltage operation, demonstrating the efficiency of voltage pulsation in improving phosphate recovery from wastewaters with simultaneous energy savings and environmental management.

# 1.1. Materials

The test solutions consisted of 10 mM NH<sub>4</sub>H<sub>2</sub>PO<sub>4</sub> with appropriate amounts of NH<sub>4</sub>Cl and (NH<sub>4</sub>)<sub>2</sub>SO<sub>4</sub> as background concentrations so that the total ammonium and phosphate concentration in the solution corresponded to 405 and 320 ppm, respectively. Milli-Q water (18.2 MΩ, Millipore, Bedford, MA, USA) was used for preparing the solutions. The composition of wastewater was chosen based on the water sample taken from a biological nutrient removal wastewater treatment plant (Garver, USA). The aqueous solutions were initially maintained at pH 7. All chemicals and 99.9 % pure Mg disc electrodes (diameter = 0.5 cm) were purchased from Sigma-Aldrich and Metal Sample (USA), respectively. Plates of 99.9 % pure Mg (99.9 % pure) and stainless steel (316SS) with surfaces of 6 cm $^2$  × 4 cm $^2$  and 0.2 cm thick were obtained from Goodfellow, USA. The Ag/AgCl reference electrode in 3.0 M NaCl was bought from BASi, USA. After each experiment, the pH of the aqueous solutions was determined in-situ using a Thermo Scientific Orion Star A111 pH meter.

### 1.2. Instrumentation and reactor setup

Using pure magnesium discs, linear sweep voltammetry (LSV) measurements were performed between -2.2 and +0.56 V vs Normal hydrogen electrode (NHE). Each disc electrode was mechanically polished with Norton Abrasives abrasive papers and then thoroughly cleaned with Milli-Q water before experiments. In a three-electrode cell equipped with a water jacket (Pine Research, USA), experiments were conducted in 30 mL of NH<sub>4</sub>H<sub>2</sub>PO<sub>4</sub> and NH<sub>4</sub>Cl/(NH<sub>4</sub>)<sub>2</sub>SO<sub>4</sub>. A graphite rod (L<sub>immersed</sub> = 2.3 cm, Ø = 0.7 cm) was used as the counter electrode. Throughout the experiment, the electrochemical cell was connected to a Gamry Instrument G3000-30111 potentiostat/galvanostat (Gamry Instruments, USA). For recording the voltammograms, a scan rate of 1 mV. s $^{-1}$  was selected, and data acquisition was performed with Gamry Framework (Version 7.8.1).

The batch experiments were conducted in a single-compartment reactor with a solution volume of ~450 mL, stirring continuously at 275 rpm. There was a 5 cm inter-electrode distance between the cathode (316SS) and anode (pure Mg) and both electrode surfaces had a maximum active surface area of 40 cm<sup>2</sup> (note both anode surfaces were used). In Fig. 1, a schematic of the setup and the formation of the passivating layer is shown. The magnesium potentials were measured against the reference electrode placed adjacent to the anode (1.5 cm) while being controlled with a VSP-300 multichannel potentiostat (Biologic, USA). The effect of frequency (0.1, 1, 10, and 100 Hz) on the performance of the reactor was investigated using test solutions at pH 7, and appropriate potentials were picked out from the LSV study. The batch experiments were conducted at these potentials during a 2-h period at room temperature, and the composition of the precipitate was analyzed for variations in magnesium/phosphorus ratios and phosphate recovery.

# 1.3. Sampling and material characterization

The grab samples (10 mL) were collected, filtered, and analyzed for Mg and P content immediately after each batch experiment. Using HACH Molybdovanadate reagent (HACH method 8114) and a DR900 multiparameter portable colorimeter (Loveland, CO, USA), the

phosphate concentration was measured by colorimetry. Precipitates from the test solution were vacuum filtered through PTFE un-laminated membranes, pore sizes 0.45 m and 47 mm, manufactured by Sterlitech, USA, and anode precipitates were gently scraped off with a razor blade. The precipitates from the bulk solution post filtration were oven dried, weighed on the Mettler Toledo, XSE105 Dual Range analytical balance, and stored for characterization.

X-ray diffraction (XRD) was used to examine the crystal structures of the precipitates on a Philips PW1830 double system diffractometer with a Cu cathode. A scanning electron microscope (SEM) was used to investigate the precipitate morphology further (FEI Nova Nanolab 200 Dual beam). Ion chromatography (IC) analysis was used to determine the  $\rm Mg^{2+}$ ,  $\rm NH_4^+$ , and  $\rm PO_3^{4-}$  compositions of precipitates and spent solutions using a dual channel Thermo ICS-6000 ion chromatography system (ThermoFischer Scientific, USA). The cations were calibrated with the IC-CAT6 standard and separated on a CS12A column with KOH eluent, whereas the anions were calibrated with the IC-2 standard and separated on an AZ19 column with methane sulfonic acid (MSA) eluent. Prior to IC analysis, all samples were filtered with a syringe filter (Acrodisc LC-25 mm) equipped with a 0.2  $\mu$ m polyvinylidene fluoride (PVDF) membrane (High performance liquid chromatography, HPLC certified) from Pall Corporation, USA.

# 2. Calculations

All potentials from the voltammograms were quoted against NHE and calculated as follows:

$$E_{\text{NHE}} = E_{\text{Ag/AgCl}} + 0.21$$
 (6)

where  $E_{\rm Ag/AgCl}$  is the measured working potential at rt 25 °C [17].

According to Faraday's law of electrolysis, the theoretical Mg dissolution from the anode based on the observed current ( $m_{\text{Mg,theo}}$ ) can be determined using the following equation [17]:

$$m_{\rm Mg,theo} = M_{Mg} \frac{Q}{zF} \tag{7}$$

where z is the  $Mg^{+2}$  valency (z = 2); Q is the electric charge in Coulomb,

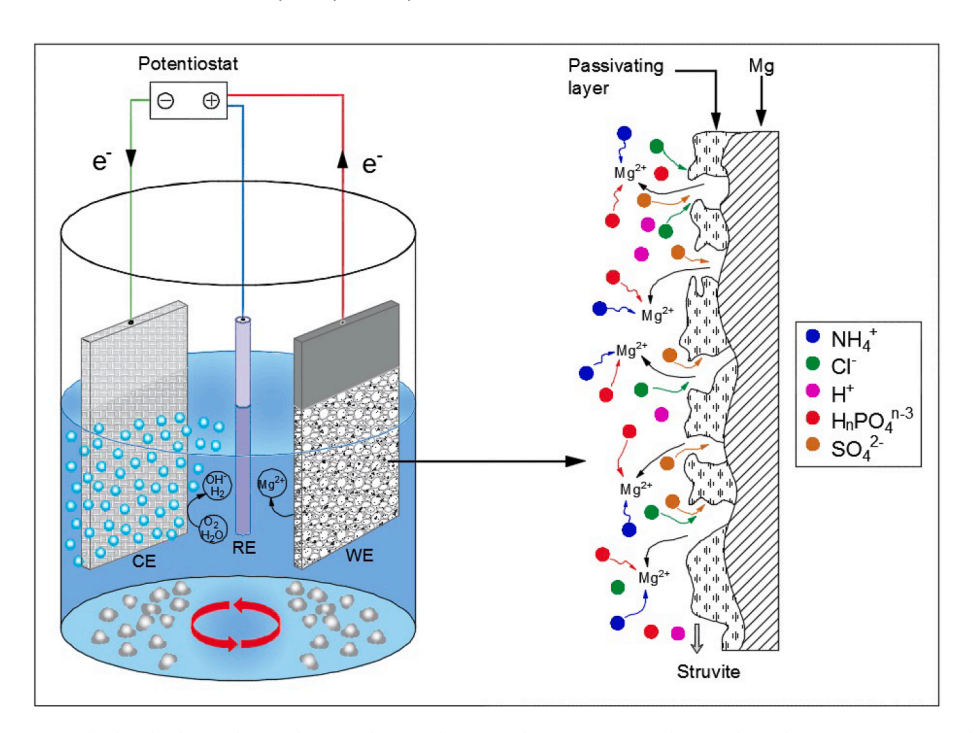


Fig. 1. Schematic illustration of the batch electrochemical setup (left) and struvite layer formation during electrolysis. CE = counter electrode, RE = reference electrode, and WE = working electrode.

obtained from  $Q = \int_0^T i(t)dt$ ; i(t) is the current profile;T is the time of each experiment; F is Faraday constant (96,485C.mol<sup>-1</sup>);  $M_{\rm Mg}$  is the Mg molar mass (24.3 g.mol<sup>-1</sup>).

The mass of dissolved Mg ( $m_{Mg,dissolved}$ ) was calculated from the IC results according to [25]:

$$m_{Mg,dissolved} = \Sigma \mathbf{M}_{i} \mathbf{w}_{Mg}^{(i)} \tag{8}$$

Where i (=1, 2, and 3) represents the bulk precipitate and anode precipitate, respectively, in the spent solution.  $M_i$  and  $w_{Mg}^{(i)}$  are the mass and corresponding weight fraction of Mg in the  $i^{th}$  phase.

The energy consumption was calculated using the following equation:

$$U_{input} = \frac{\int E(t)I(t)dt}{m_p} \tag{9}$$

where  $U_{\text{input}}$  is the theoretical energy consumption in KWh.kg<sup>-1</sup>, E and I are the cell voltage (V) and current (A) at time t and  $m_{\text{p}}$  is the precipitate mass after 2 h batch electrolysis.

The nutrient (phosphate and ammonia) recovery efficiency was calculated immediately after each batch experiment using the following equation [51]:

$$N_{Rec} = \frac{(C_i - C_t)}{C_i} \times 100\%$$
 (10)

where  $N_{Rec}$  is the nutrient recovery efficiency (%) for phosphate (PO $_{Rec}^{3-}$ ) and ammonium (NH $_{Rec}^{+}$ ) ions,  $C_t$  is the initial (t=0) nutrient concentration (mg.L $^{-1}$ ), and  $C_t$  is the phosphate concentration at time t (mg.L $^{-1}$ ).

The total hardness was calculated as the equivalent of calcium carbonate (CaCO<sub>3</sub>) by using equation below [52]:

$$TH[CaCO_3] = 2.497 \times [Ca^{2+}] + 4.12 \times [Mg^{2+}]$$
 (11)

where TH denotes total hardness as  $CaCO_3$  (mg.L<sup>-1</sup>),  $[Ca^{2+}]$  represents calcium ion concentration, and  $[Mg^{2+}]$  implies magnesium ion concentration, both in mg.L<sup>-1</sup>.

# 3. Results and discussion

# 3.1. Electrochemical characteristic of pure Mg anode

The very negative equilibrium potential of Mg/Mg<sup>2+</sup> ( $E_{MMg}^{2+} = -2.128$  V vs NHE) gives rise to the negative difference effect (NDE), which has been linked with the localized anodic dissolution of the magnesium metal and an increase in hydrogen evolution at the pitting potential [29,51,53]. However, the electrochemistry of magnesium metal is complex, and there is disagreement over the corrosion and passivation processes of magnesium [54,55]. Therefore, we performed linear sweep voltammograms to evaluate the electrochemical characteristics of magnesium electrodes in chloride and sulfate containing phosphate solutions.

Fig. 2 shows the electrochemical behavior of the magnesium disk electrode in the potential range of -2.2 V vs NHE to +0.56 V vs NHE at rt. Representative voltammetry curves exhibit steep increases in current in the positive voltage regions for the expected hydrogen evolution reaction (HER) [56]. The shifts in the curve upon changing electrolyte composition could be due to the dynamically changing electrode surface during the experiment, where the passivation induced solids produced on the magnesium accumulate, altering the electrochemical kinetics and overall rate of the electrochemical reactions. The corrosion potential  $(E_{corr})$  occurs at -1.98 V and -1.52 V vs NHE in presence of Cl $^-$  and  $SO_4^{2-}$  ions, respectively. The current density, thereafter, increases slowly with voltage. However, at the corresponding pitting potentials  $(E_{pit})$  of -1.05 V and -0.63 V vs NHE, corrosion of the electrode material occurs via pit formation on the surface of the electrode, and this activation

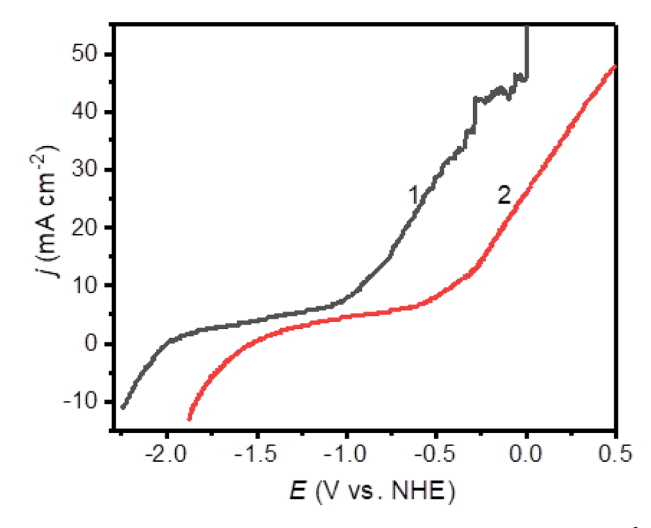


**Fig. 2.** Linear Sweep Voltammetry (LSV) analysis performed at 1 mV s<sup>-1</sup> to identify mean anode potential ( $E_{\rm m}$ ) in (1) chloride and (2) sulfate containing test solutions.

causes a sharp increase in the current density. The higher rate of increase in  $\frac{\partial j}{\partial V}$  in the chloride containing solution may indicate an increased degree of passivation layer rupture, particularly because  $Cl^-$  have been reported to depassivate the electrode surface layer more than  $SO_4^{2-}$ , which could in turn speed up the dissolution of the surface film [29,53].

Interpretation of the voltametric profiles and other experimental outcomes requires the understanding of passivation layer dynamics in relation to the changing electric field. The dynamics of passivation layer may be described in terms of (i) initial formation and growth, (ii) partial rupture at  $E > E_{corr}$ , and (iii) increased rate of rupture beyond  $E_{pit}$ . In an aqueous environment, immediately after immersion, a thin film of MgO (<25 Å) forms on the surface of Mg electrode, which is further covered by a growing Mg(OH)<sub>2</sub> layer [57]. Corresponding XPS analysis indicated the growth of the Mg(OH)2 layer to tentatively saturate at 10 nm after 120 s. The compact MgO-Mg(OH)<sub>2</sub> bilayer, commonly referred to as the "passivation layer", is fundamentally responsible for making the Mg electrode electrically inert over the potential range between  $E_{corr}$  and  $E_{pit}$ . This may be confirmed by low charge transfer (1–3 mA.cm<sup>-2</sup> and 0.5–1.2 mA.cm<sup>-2</sup> for Cl<sup>-</sup> and SO<sub>4</sub> containing solutions, respectively) over the same potential range. However, once the applied potential crossed  $E_{\text{pit}}$ , charge transfer was noted to increase as the respective Maxwell stress  $\left( = \frac{1}{2} \varepsilon E^2 \right)$ , where  $\varepsilon$  is the permittivity and E is the field strength is apprehended to exceed the ultimate stress of the MgO-Mg(OH)<sub>2</sub> bilayer causing partial layer rupture. The bilayer rupture immediately caused direct exposure of Mg electrode with the electrolyte over some regions of the electrode and the release of  $Mg^{+2}$  was initiated. The release rate progressively increased with the applied voltage, which is marked by the monotonic trend of j versus E profile (Fig. 2). The increased release of Mg<sup>+2</sup> could lead to higher rates of electrolytic product formation (primarily struvite), which may precipitate on the ruptured area, reducing the rate of charge transfer and Mg<sup>+2</sup> release. Nevertheless, the phenomenon could not be captured by voltammetry because of the constant increase of potential. The overall mechanism is schematically presented in Fig. S1.

The determination of the  $E_{\rm pit}$  is important because previous electrochemical investigations, carried out in our group, have demonstrated stable operation of the electrochemical system at voltage s >  $E_{\rm pit}$  [32,58]. Furthermore, considering our primary objective to investigate the efficacy of pulsating anode potential to promote rupture of the passivating layer, we have chosen  $E_{\rm pit}$  as the mean potential (= $E_{\rm m}$ ) and set the amplitude (A) to 0.5 V to maintain the minimum potential (= $E_{\rm m}$ -A) higher than  $E_{\rm corr}$ .

# 3.2. Electrolysis

We have primarily focused on the chronoamperometric profiles (j versus t plots) of the batch experiments to understand the fundamental characteristics of the input-output relation. Fig. 3 displays the evolution of current density with time for the pure magnesium electrode in different compositions of the phosphate solution. The standard theory of Frequency Response Analysis (FRA) predicts that a system with a sinusoidal input function will generate a sinusoidal output after a brief initial transient [59]. Consistent with the general prediction of FRA, the transient profile of current density displays sinusoidal variation in all cases. Nevertheless, the respective current density bandwidth changes significantly with composition and frequencies. Moreover, for individual frequencies, the bandwidth also changes with time. For example, in chloride phosphate solution, a change of frequency from 0.1 Hz to 100 Hz results in an initial change of bandwidth from 11.0 to 0.05 mA cm<sup>-2</sup>. On the other hand, at f = 1 Hz, the sulfate phosphate solution exhibits a bandwidth variation from 8.0 mA cm<sup>-2</sup> at  $t = 0^+$  h to 5.5 mA cm<sup>-2</sup> at t =2 h. In general, the current density bandwidth increases over 0.1–1 Hz and decreases at higher frequencies of 10-100 Hz. The diminishing bandwidth of *i* with frequency indicates a frequency range over which the effect of potential pulsation on the overall response is significant. The effect of such pulsation is negligible at 100 Hz, which possibly implies a mismatch of order between the corresponding time-scales (i.e., the time scale of voltage pulsation ≪ time-scale for Mg<sup>2+</sup> dissolution and transport from the anode surface to bulk).

For each frequency, the higher j values at  $t = 0^+$  h for chloride solution suggest increased pitting corrosion in saline solutions. However, the gradual decrease of the mean current density can be attributed to the blockage of initial film free areas of Mg anode by the electrolytic product that most likely consisted of struvite. At the pitting potential, the reduction of water molecules to H<sub>2</sub> and OH<sup>-</sup> occurs [17,53,60]. The hydroxyl ions accumulation resulted in a pH rise and influenced the stability of the insulating layer on the magnesium surface [23,25,32,61]. For all frequencies, the lower *j* values in sulfate solution may indicate a reduced degree of passivation layer rupture than in chloride solution. The effect of voltage pulsation on the passivation layer is quite similar to the 'early' failure of thin film subjected to pulsating mechanical stress. Early rupture (i.e., at lower mean stress compared to constant stress experiment) of such film under pulsating stress is commonly referred to as 'fatigue' [62]. The present work is an apprehensive extension of mechanical fatigue to Maxwell stress regime. For a sinusoidal voltage pulsation (i.e.,  $E=\overline{E}+ASin\omega t$ ), the corresponding Maxwell stress becomes a quadratic periodic function  $\left[=\frac{1}{2}(\overline{E}+ASin\omega t)^2\right]$ . By applying a pulsating anode potential, the passivation layer subjected to pulsating Maxell stress may rupture early, resulting in more precipitate formation through the transverse cracks.

The transients for the control (constant voltage hold) experiments, as shown in Fig. S2, show a gradual decrease in current density over time and drop to j values of 4.0 mA cm $^{-2}$  and  $\sim$ 1.0 mA cm $^{-2}$  in chloride and sulfate solutions, respectively at the end of the experiment. Once the insulating film forms on magnesium, precipitation occurs through filmfree areas. However, with time, further precipitation may block the active sites of the electrode causing a decrease in current density. The abrupt increase in currents at times of about 0.65 h, and 1.75 h in 1 Hz chloride solution, and at 0.6 h in 0.1 Hz sulfate solution could signify disintegration of the anodic material into the bulk solution due to spalling or hydrogen evolution at the anode. Although the transient profiles at 100 Hz exhibit characteristics typical of the voltage-hold experiments, higher j values are obtained in the pulsating potential experiments, which elevate the theoretical Mg release ( $m_{\rm Mg,theo}$ ) by 17 % in  $\rm Impact Mg$  in  $\rm Impact Mg$  and  $\rm Impact Mg$  in  $\rm Impact Mg$  and  $\rm Impact Mg$  in  $\rm Impact Mg$  and  $\rm Impact Mg$  in  $\rm Impact Mg$  in  $\rm Impact Mg$  and  $\rm Impact Mg$  in  $\rm Impac$ 

Precipitates recovered after 2 h were greater in dynamic potential experiments (as opposed to constant voltage) and the results are

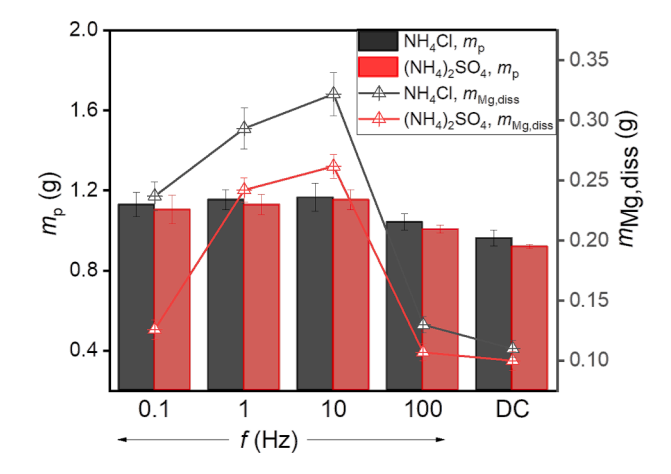


Fig. 4. The mass of precipitates  $(m_p)$  and dissolved magnesium mass  $(m_{Mg,diss})$  obtained under various frequency conditions at initial pH 7.

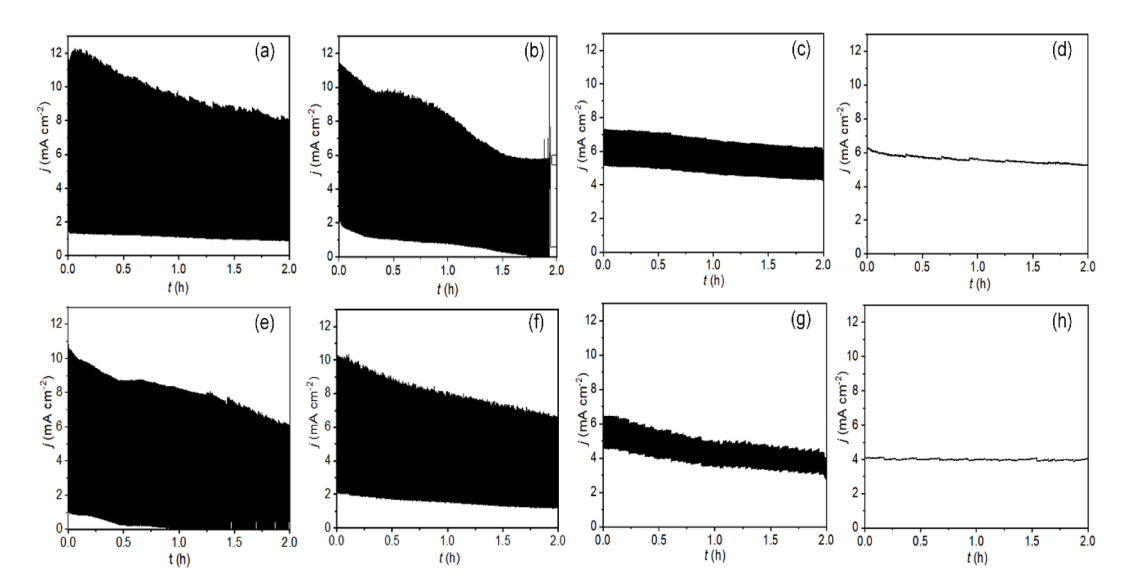


Fig. 3. The changes in the current density over 2 h for pulsating potential experiments with frequency values of 0.1–10 Hz in (a-d) chloride and (e-f) sulfate solutions. The respective frequency values are 0.1 Hz (a,e); 1 Hz (b,f); 10 Hz (c,g); and 100 Hz (d,h).

presented in Fig. 4. In our overall measurement of struvite recovery, we do not account for any dissolved, solubilized struvite remaining in saturated aqueous solutions. Though we do not account for solubilized struvite particles, struvite recovery processes could only recover formed particles. We believe that focusing on particulate struvite as the recoverable portion is relevant to an engineered wastewater treatment process, and we are not overestimating the recovery potential of struvite by including a solubilized struvite contribution as well.

Similar to our previous batch experiment study with ammonium dihydrogen phosphate and chloride solution, no precipitate was observed on the cathode, and struvite formed exclusively in the bulk solution [25]. Negligible amount of precipitate was formed on the anode surface and the mass values are reported in Table S1. The difference in the thickness of the surface film on the electrodes or the precipitate collection method could explain the slightly higher precipitate mass on the anode in sulfate solution at 100 Hz and control. A straight razor was used to gently scrape the precipitate off the plate, where some excess pure Mg particles from the plate could have artificially elevated the mass of electrode precipitate.

The lowest precipitate mass  $(m_p)$  in solution was obtained from the control experiments, while the highest mass was recorded in the pulsed potential experiments conducted at 10 Hz. When compared to the control experiments, the production of dissolved  $Mg^{2+}$  ( $m_{Mg,diss}$ ) in chloride solution increased by 21 % (100 Hz)-196 % (10 Hz), which resulted in ca. 8.5-27 % more precipitate mass formation (Fig. 4). Similarly, the sulfate solution exhibited 9.3 % (100 Hz)-25.3 % (10 Hz) improvement in precipitate yield compared to the control experiment. When supporting electrolytes (i.e., chloride and sulfate) are present with the phosphate solution, differences in conductivity may affect the current density, voltage, and precipitation yield. Upon applying an electric field, Mg<sup>2+</sup> is released as a result of both theoretical Mg releases predicted by Faraday's law, and additional Mg releases during HER on the anode. As a result of the negative difference effect (NDE), HER accelerates during anodic polarization in electrolysis reactors, so the total number of electrons participating in electrode surface reactions is the sum of electrons applied from external potentials (or currents) and electrons from HER [16]. Accordingly, chloride and sulfate ions may enhance Mg corrosion and consequently enhance hydrogen production on electrode surfaces. Due to the formation of hydrogen bubbles, the electrolyte may be prevented from accessing the surface of the electrode, thereby reducing the electrode's active surface area [34]. However, the application of pulses may force the detachment of the bubbles from the electrode surface and improve mass transport conditions.

When comparing the proposed technique to conventional constant voltage batch electrolysis, economic analysis plays a significant role in determining the potentiability of the proposed technique. Evaluation of the theoretical energy consumption, according to Eqn. (9), shows that the chloride based system consumed 9–14 % lower energy across all frequencies (Fig. 5) compared to the sulfate solution. The changes in  $U_{\rm input}$  with f and ionic make-up is presumably due to the differences in electrode film formation and ionic magnesium release, factors which can in turn be affected by charge density and the presence of  $Cl^-$  and  $Cl^-$  ions (Table S2). At 10 Hz, the energy consumption decreased by 8 % and  $Cl^-$  and  $Cl^-$  ions (Table S2); an explanation for the dramatic decrease in energy value in presence of sulfate may come from a larger increase in mean  $Cl^-$  ions a comparatively smaller change in  $Cl^-$  by 1.2x.

Profiles of PO<sub>4</sub>-P and NH<sub>4</sub>-N recovery for the pulsating frequencies and controls are illustrated in Fig. S3, where the reported values represent the average results from three duplicate measurements. All profiles are noted to pass through maxima at 10 Hz in the two different test solutions (Fig. S3a). However, the respective profiles in chloride containing solutions were always higher than those of sulfate containing solutions. Both phosphate and ammonium recovery accelerated with increased frequency until 10 Hz due to higher production of Mg<sup>2+</sup> to promote precipitation. The phosphate recovery in chloride solution

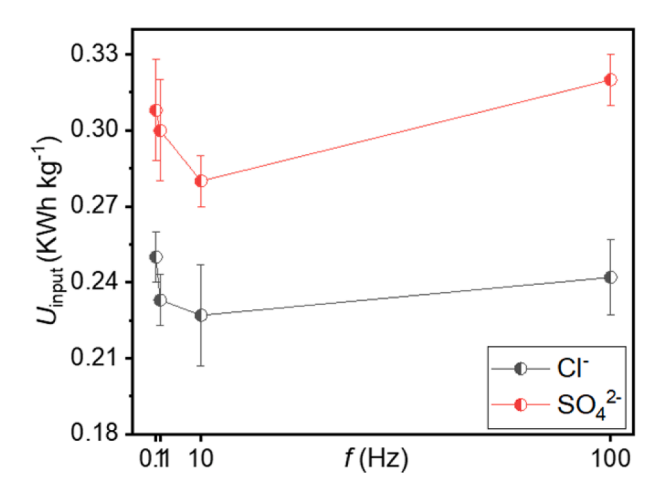


Fig. 5. The theoretical energy consumption evaluated as per kg of precipitate obtained.  $m_0$ 

improved from 78.3  $\pm$  4 % in control to 95  $\pm$  6 % at 10 Hz but dropped to 85  $\pm$  4 % at 100 Hz (Fig. S3b), indicating more exhaustive reactions in the pulsating potential driven system. A similar trend was observed for ammonium ions, nevertheless, the recovery for ammonium (ca. 32 % at 10 Hz) was much less than phosphate. The discrepancy arises from the initial ammonium concentration being 1.3x higher than the initial phosphate concentration. However, based on the ratio of their absolute concentration decrease, the ammonium and phosphate have a 1:1 recovery ratio, which is consistent with the theoretical stoichiometric ratio of struvite.

The minimum struvite solubility occurs at pH 8.8-9.7 [10,13,63]. With the increase in applied frequency, pH in both solutions increased due to generation of hydroxyl ions near the electrodes (as described in Eqs. (3), (4) and (5)) and exceeded pH 9.4 at t = 2 h, which is conducive to Mg(OH)2 and other magnesium phosphate based compound formation (Table S1) [17,32,58]. The increase in pH of the bulk solution would further produce a shift of ammonium ions to ammonia and release NH<sub>3</sub> into the surrounding atmosphere [32,64]. Further, during electrode corrosion and magnesium dissolution, the pH of the bulk solution and the near-anode solution may be affected by changes in ion speciation, which in turn may influence water chemistry effects on anode corrosion as well as precipitation. A previous study by the author also showed an increase in solution pH by ~2.5 units post 2 h of operating the batch reactor [25]. Therefore, in this study, we have limited the electrolysis time (i.e., 2 h) to minimize ammonia volatilization and precipitation of Mg(OH)<sub>2</sub> and other magnesium phosphate compounds, which would reduce the purity of the electrochemically obtained struvite. The present trend of pH variation suggests pH control at 9.0 to maximize pulsating induced struvite precipitation which has been attempted from a natural municipal wastewater (MWW) sample as discussed in Section 4.4. The intermittent time for a batch reactor can generally be determined by recording chronoamperometric transients (i. e., measuring the variation in current over time) in the previously described electrochemical cell, where the current density is expected to decrease slowly and reach a low steady state. Despite this, it is pertinent to note that a steady state cannot be achieved in the present system due to a dynamic process of precipitate building up and passivation layer rupture occurring simultaneously.

# 3.3. Precipitate characteristics

After the 2-h batch experiments, SEM characterization was employed to determine the surface morphology of the magnesium electrodes. For this specific study, the precipitated crystals were left on the electrodes and carefully stored so that the originally formed crystal structure was not altered during sample processing post-experiments. Fig. 6 shows

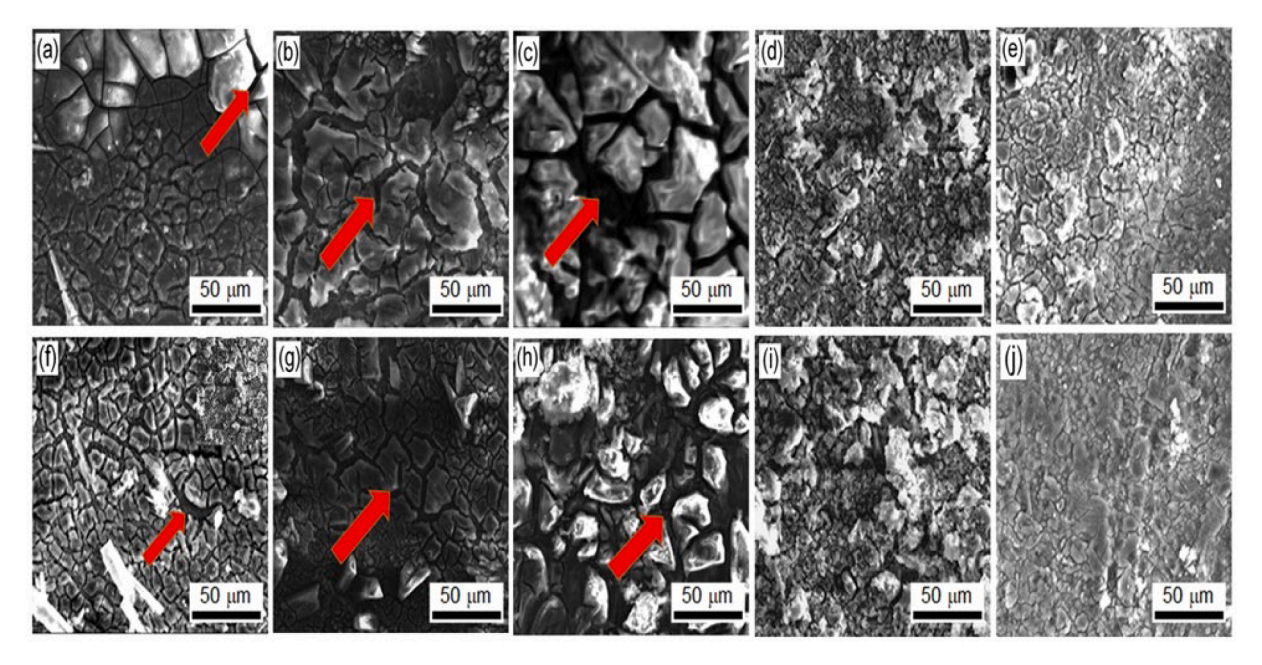


Fig. 6. SEM images of the precipitate layers produced on Mg anodes in solutions with (a-e) chloride and (f-j) sulfate ions with (left–right) 0.1, 1, 10, 100 Hz pulsating potential frequencies and constant voltage conditions.

SEM micrographs of precipitates formed in chloride and sulfate solutions at a magnification of 50x. The anode surface did not show any significant precipitation at lower frequencies of 0.1–10 Hz, and irregular and uneven surface cracks on the magnesium plates were observed. Formation of deeper cracks (shown with red arrows in Fig. 6) could imply higher availability of the electrode's active surface to the electrolyte leading to more severe corrosion, which is in accordance with the  $m_{\rm Mg,diss}$  and precipitate mass values reported in Fig. 4. The morphology of the precipitates in bulk solution in chloride medium display needle-like elongated structures with predominantly smooth surfaces and sharp edges (Fig. S4a–d), as reported by other researchers, suggesting the precipitates are composed of struvite crystals [12,13,32,65,66]. A change in the constitution of the test solution may have resulted in crystal aggregates as seen in sulfate solutions (Fig. S4f–i).

Qualitative elemental mapping of <sup>24</sup>Mg of magnesium anode post

electrochemical experiments was done by laser ablation ICP-MS. The anodes in chloride solution (Fig. 7a–e) showed a relatively higher abundance of magnesium in comparison to sulfate solutions (Fig. 7f–i) in both pulsating potential and control experiments. The highest magnesium intensities were recorded on the metal electrodes subjected to the frequency of 10 Hz. These results are in consistent with the Mg<sup>2+</sup> release profiles discussed in section 4.2. The relatively low intensities of elemental Mg on anodes in sulfate solution is likely due to the less 'invasive' pitting action of sulfate as compared to chloride ions. The differences in pitting morphology can be associated with different distribution of the Mg atoms on the electrode surface and may be dependent on the solution composition and applied frequency.

The atomic percentages (at %) of the corresponding elements from the recovered precipitate were determined using EDX to provide qualitative analysis of elements distribution within a micro area of the Mg

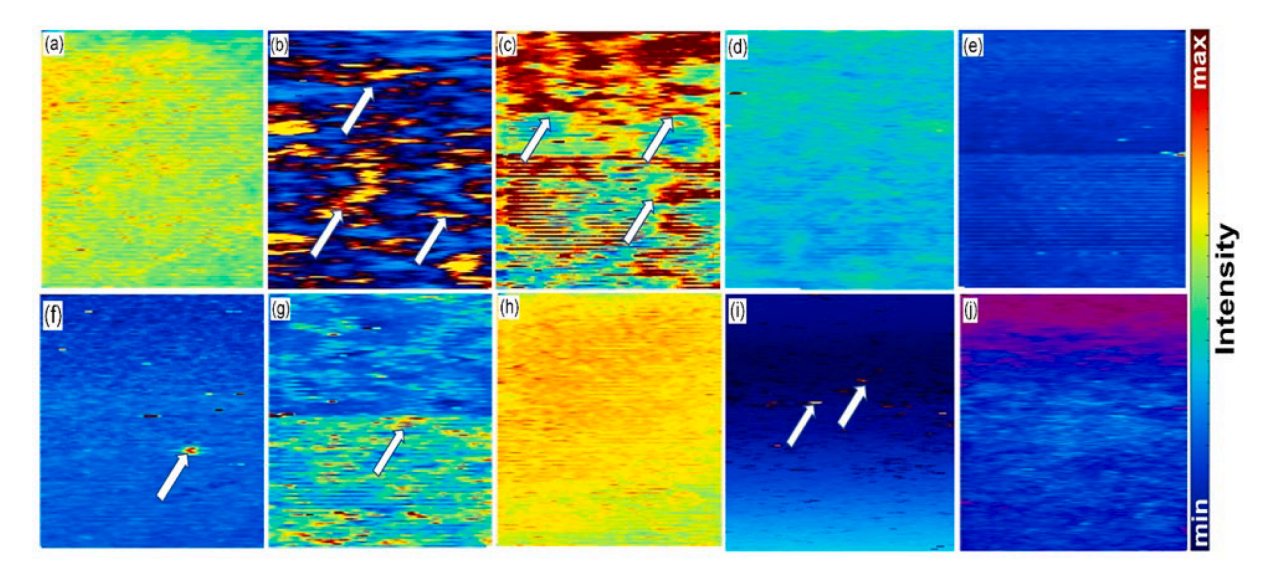


Fig. 7. LA-ICP-MS distribution of <sup>24</sup>Mg on used magnesium anodes after the (a-d, f-j) pulsating potential and (e,f) dynamic potential experiments in order of increasing frequency. The electrodes (a-e) and (f-j) were used in the electrochemical reactor containing chloride and sulfate solutions respectively. The white arrows represent pits on the electrode surface.

surface (Fig. S5). The EDX spectra for both anode and bulk precipitates show prominent peaks for Mg, P, and N usually present in electrochemically precipitated struvite crystals. The precipitate from the anode surface was gently scrapped off to eliminate the interfering effects of Mg substrate on the EDX spectra. The at % ratio of Mg/N increased with frequency between 0.1 and 10 Hz and then drops to lower values at 100 Hz (Fig. S6a). The deviation from a theoretical ratio of 1.0 can be attributed to the presence of less ammonium in the films due to higher pH conditions near the anode [23]. Similarly, the higher ratios of Mg/P in the chloride system (Fig. S6b) can be explained is possibly due to increased Mg dissolution as supported by the  $m_{\rm Mg,diss}$  values as shown in Fig. 4. The elemental mapping of the precipitates revealed a homogenous distribution of the significant elements (Mg, P, and N) in the surface films (Fig. S7).

Based on XRD analysis of the electrochemically produced struvite (Crystal Green), it was found that the peak intensity of the electrochemically produced struvite was similar to the chemically precipitated struvite (Fig. S8). A difference in peak intensities could indicate that the precipitate has a different structure than struvite available commercially. Additional diffraction peaks of magnesium, Chloromagnesite (magnesium chloride), and Mg(OH) $_2$  were detected in anode precipitates when chloride was added (Fig. S8c–g), whereas peaks of newberyite ((Mg(PO $_3$ OH).3H $_2$ O) were observed in the sulfate system at 0.1,1, and 100 Hz and in the control system (Fig. S8h–l). However, based on the characterization results, we believe the precipitates collected from the reactor were first and foremost struvite.

### 3.4. Nutrient removal from a municipal wastewater

As a next step, the feasibility of nutrient removal from a natural wastewater source using dynamic potential was examined. For this purpose, optimum struvite precipitation conditions were used (i.e.,  $E_{\rm mean} = -1.03~{\rm V}$  vs NHE and  $f = 10~{\rm Hz}$ ). The raw wastewater sample was pretreated with a crossflow membrane filtration system to remove suspended solids that may foul the Mg anode, and the composition of the pre-treated and post-experiment municipal wastewater (MWW) samples are provided in Table S3 (NB: detailed description of the pre-treatment step is provided in the Supporting Information). The solution pH was maintained at 9.0 as in a real-world scenario surface water pH is typically between 6.5 and 8.5, and higher pH levels would require an additional pH adjustment step in wastewater treatment plants [33]. In addition, the performances of the reactor as well as the total hardness and energy input were evaluated and compared with a constant voltage system (Table 1).

A 1.2x higher energy input for nutrient removal resulted in 90.1 and 17.3  $PO_4^{3-}$  and  $NH_4^+$  recovery efficiencies under constant voltage. The dynamic voltage experiment, on the other hand, exhibited a remarkable 95.2 %  $PO_4^{3-}$  recovery. Since the MWW sample has 11x higher ammonium concentration (40 ppm) than that of phosphate (3.6), the latter was limiting component in the struvite precipitation reaction. It is also suggested that pH is an important factor when it comes to the removal of  $PO_4^{3-}$  because in alkaline solutions the  $PO_4^{3-}$  (HPO $_4^{3-}$ /PO $_4^{3-}$  pKa = 12.67) form dominates [67–69], while indirect oxidation by an oxidation

**Table 1** The calculated energy consumption ( $U_{\text{input}}$ ); nutrient recovery efficiency ( $N_{\text{Rec}}$ , %); initial total hardness ( $TH_{\text{f}}$ ); and final total hardness ( $TH_{\text{f}}$ );

Electrolysis type	Energy consumption (KWh $kg^{-1}$ ) <sup>a</sup>	(PO <sup>3-</sup> <sub>Rec</sub> , %) <sup>b</sup>	(NH <sub>Rec</sub> , %) <sup>b</sup>	<i>TH</i> ₁ <sup>c</sup>	<i>TH</i> <sub>f</sub> <sup>c</sup>
Pulsating potential	0.29	95.2	19	84.9	217.7
Constant voltage	0.35	90.1	17.3	84.9	200.2

a energy consumption determined from Eq. (9).

mediator such as HOCl or  $OCl^-$  (pH = 7) produced on the anode surface could account for the low ammonia recovery [70]. Additionally, the elevated pH near the anode may also cause ammonia loss due to volatilization. The TH of the pre-treated wastewater was classified as slightly hard (84.9), while  $Mg^{2+}$  release in the solution elevated the *TH* (note: there was no measurable  $Ca^{2+}$  loss through precipitation) by  $\sim 2.5x$  post experiment and placed the water samples in the hard water classification (Table S3). The 8.5 % increase in TH after the application of pulsating potential can be correlated to the 19.8 % improvement in Mg<sup>2+</sup> dissolution into the solution. Although the TDS increased due to the changes in the Mg<sup>2+</sup> and Ca<sup>2+</sup> concentration in the system, the water quality post experiment improved with lower TOC, TOD, K<sup>+</sup>, Na<sup>+</sup>, NO<sub>3</sub> and SO<sub>4</sub><sup>2-</sup> levels. Additionally, the obtained SEM images and XRD spectra show that phosphate is primarily recovered as struvite (Fig. 8). However, closer investigation also reveals presence of magnesium hydroxide and magnesium phosphate based precipitates in the recovered spectra (Fig. S9). Other probable P removal pathways could be electrocoagulation due to metal impurities (i.e., aluminum and iron) in Mg metal (N.B. 70 mg.L<sup>-1</sup> Al and 280 mg.L<sup>-1</sup> Fe are present in Mg electrode based on the specification provided by the vendor); during corrosion, these metals could dissolve into the wastewater. Microorganisms and bacteria present in wastewater may also offer an alternative pathway for biological P removal. Furthermore, struvite precipitation is limited by phosphate, and due to the high ammonia concentrations, ammonia will likely remain even after all phosphate has been removed [33].

As a result of treating P as a contaminant, traditional chemical and biological processes for removing P consume less energy than P recovery processes, but all of the P removed is lost as solid waste, which is often disposed of in landfills [71–73]. This is one of the major drawbacks of the existing processes. As a result, P recovery processes provide a new way to rethink wastewater treatment as a resource recovery process; however, technological development and adoption will be influenced in part by energy consumption concerns. As such, our studies of electrochemical struvite precipitation using a novel pulsating potential with a sinusoidal waveform approach suggest that this is a more energy efficient technology, particularly at lower frequency values ( $\leq$ 10 Hz).

# 4. Conclusions

In summary, we show the feasibility of struvite precipitation electrochemically at lower energy requirement upon varying the voltage with a sinusoidal waveform at different frequencies. The pulsating potential-based experiments outperformed control experiments performed at fixed voltage in terms of higher phosphate recovery and struvite mass. Pulsation was less pronounced at higher frequencies, resulting in a uniform and compact foulant layer on the anode. In contrast, a porous surface film formed at lower frequencies with 96 %  $PO_4^{3-}$  and ~50 % NH<sub>4</sub><sup>+</sup> recovery efficiencies. A variety of surface characterization techniques have determined the anode surface to contain struvite of high quality. The reactor was also tested under realistic conditions, in which 95.2 % of the H<sub>n</sub>PO<sub>4</sub><sup>n-3</sup> present in municipal wastewater was primarily removed as struvite. However, for electrochemical struvite production, pulsating electrolysis must be evaluated on a larger scale or at a system level. It needs to be determined whether the pulse effect is also present with larger electrodes or larger electrolytic systems before application. Future evaluations should also consider the mechanistic aspect of the pulse effect on the electrode-electrolyte interface regime in order to provide greater tuning options for conventional electrolysis.

# **Declaration of Competing Interest**

The authors declare that they have no known competing financial interests or personal relationships that could have appeared to influence the work reported in this paper.

<sup>&</sup>lt;sup>b</sup> phosphate and ammonium recovery efficiency calculated from Eq. (10).

c initial and final hardness determined from Eq. (11).

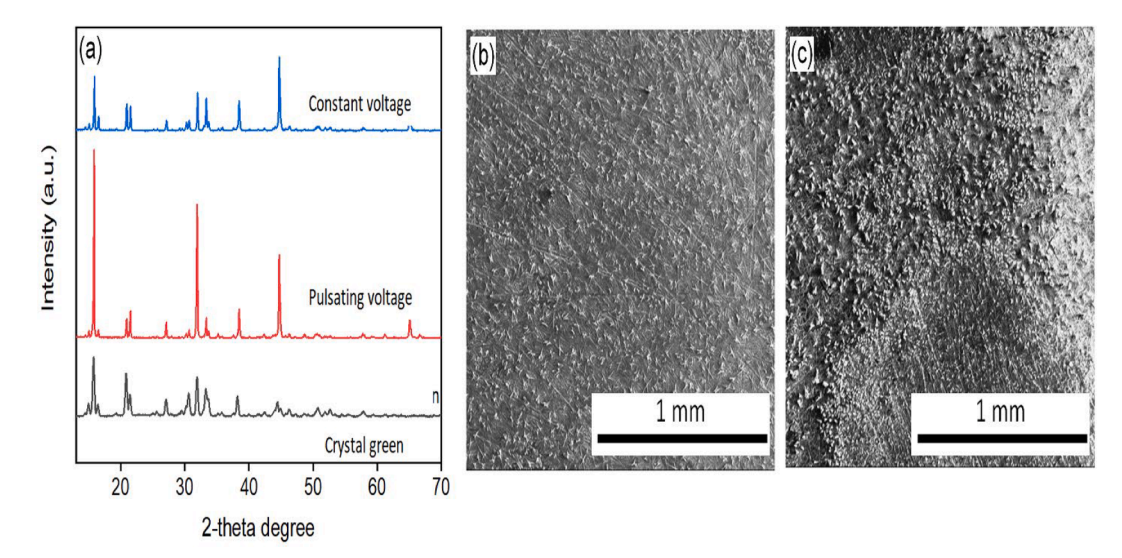


Fig. 8. (a) XRD spectra of struvite formed with pulsating and constant (control) voltage. SEM images obtained of the struvite layer formed on the anodic plate upon (b) voltage fluctuation and (c) control.

### Data availability

Data will be made available on request.

# Acknowledgements

The authors gratefully acknowledge the National Science Foundation for funding under grant #1739473, and the program Innovations at the Nexus of Food, Energy, and Water Systems. The authors also acknowledge technical support from the characterization facility at the Institute for Nanoscience and Engineering at the University of Arkansas and the Materials Characterization Laboratory at the Pennsylvania State University.

# References

- D. Cordell, J.-O. Drangert, S. White, The story of phosphorus: Global food security and food for thought, Global Environmental Change 19 (2) (2009) 292–305.
- [2] K.-L. Huang, C.-C. Liu, C.-Y. Ma, T.-T. Chen, Effects of operating parameters on electrochemical treatment of swine wastewater, Int. J. Electrochem. Sci. 14 (2019) 11325–11339.
- [3] M.J. McLaughlin, Land application of sewage sludge: Phosphorus considerations, South African Journal of Plant and Soil 1 (1) (1984) 21–29.
- [4] Z. Yuan, S. Pratt, D.J. Batstone, Phosphorus recovery from wastewater through microbial processes, Current opinion in biotechnology 23 (6) (2012) 878–883.
- [5] B.K. Mayer, L.A. Baker, T.H. Boyer, P. Drechsel, M. Gifford, M.A. Hanjra, P. Parameswaran, J. Stoltzfus, P. Westerhoff, B.E. Rittmann, Total value of phosphorus recovery, Environmental science & technology 50 (13) (2016) 6606–6620.
- [6] R. Brennan, M. Healy, L. Morrison, S. Hynes, D. Norton, E. Clifford, Management of landfill leachate: The legacy of European Union Directives, Waste management 55 (2016) 355–363.
- [7] O. Ichihashi, K. Hirooka, Removal and recovery of phosphorus as struvite from swine wastewater using microbial fuel cell, Bioresource technology 114 (2012) 303–307.
- [8] J. Driver, D. Lijmbach, I. Steen, Why recover phosphorus for recycling, and how? Environmental technology 20 (7) (1999) 651–662.
- [9] C.A. Cid, J.T. Jasper, M.R. Hoffmann, Phosphate Recovery from Human Waste via the Formation of Hydroxyapatite during Electrochemical Wastewater Treatment, ACS Sustainable Chemistry & Engineering 6 (3) (2018) 3135–3142.
- [10] M. Ronteltap, M. Maurer, W. Gujer, Struvite precipitation thermodynamics in source-separated urine, Water Research 41 (5) (2007) 977–984.
- [11] R.D. Cusick, B.E. Logan, Phosphate recovery as struvite within a single chamber microbial electrolysis cell, Bioresource Technology 107 (2012) 110–115.
- [12] M.P. Huchzermeier, W. Tao, Overcoming Challenges to Struvite Recovery from Anaerobically Digested Dairy Manure, Water Environment Research 84 (1) (2012) 34–41.
- [13] K.S. Le Corre, E. Valsami-Jones, P. Hobbs, S.A. Parsons, Impact of calcium on struvite crystal size, shape and purity, Journal of Crystal Growth 283 (3) (2005) 514–522.

- [14] J. Wilsenach, C. Schuurbiers, M. Van Loosdrecht, Phosphate and potassium recovery from source separated urine through struvite precipitation, Water research 41 (2) (2007) 458–466.
- [15] G.L. Bridger, M.L. Salutsky, R.W. Starostka, Micronutrient Sources, Metal Ammonium Phosphates as Fertilizers, Journal of Agricultural and Food Chemistry 10 (3) (1962) 181–188.
- [16] X. Tan, R. Yu, G. Yang, F. Wei, L. Long, F. Shen, J. Wu, Y. Zhang, Phosphate recovery and simultaneous nitrogen removal from urine by electrochemically induced struvite precipitation, Environmental Science and Pollution Research 28 (5) (2021) 5625–5636.
- [17] A. Hug, K.M. Udert, Struvite precipitation from urine with electrochemical magnesium dosage, Water Research 47 (1) (2013) 289–299.
- [18] E. Kirinovic, A.R. Leichtfuss, C. Navizaga, H. Zhang, J.D. Schuttlefield Christus, J. Baltrusaitis, Spectroscopic and microscopic identification of the reaction products and intermediates during the struvite (MgNH4PO4· 6H2O) formation from magnesium oxide (MgO) and magnesium carbonate (MgCO3) microparticles, ACS Sustainable Chemistry & Engineering 5 (2) (2017) 1567–1577.
- [19] D. Kiani, M. Silva, Y. Sheng, J. Baltrusaitis, Experimental insights into the genesis and growth of struvite particles on low-solubility dolomite mineral surfaces, The Journal of Physical Chemistry C 123 (41) (2019) 25135–25145.
- [20] W.A. Tarpeh, J.M. Barazesh, T.Y. Cath, K.L. Nelson, Electrochemical Stripping to Recover Nitrogen from Source-Separated Urine, Environmental Science & Technology 52 (3) (2018) 1453–1460.
- [21] M. Liao, Y. Liu, E. Tian, W. Ma, H. Liu, Phosphorous removal and high-purity struvite recovery from hydrolyzed urine with spontaneous electricity production in Mg-air fuel cell, Chemical Engineering Journal 391 (2020), 123517.
- [22] A. Xie, S.C. Popat, Electrochemical ammonia stripping from non-nitrified animal rendering wastewater, Chemical Engineering Journal Advances 3 (2020), 100020.
- [23] S.B. Moussa, G. Maurin, C. Gabrielli, M.B. Amor, Electrochemical precipitation of struvite, Electrochemical and solid-state letters 9 (6) (2006) C97–C101.
- [24] X. Lin, Z. Han, H. Yu, Z. Ye, S. Zhu, J. Zhu, Struvite precipitation from biogas digestion slurry using a two-chamber electrolysis cell with a magnesium anode, Journal of Cleaner Production 174 (2018) 1598–1607.
- [25] R. Sultana, L. Kékedy-Nagy, R. Daneshpour, L.F. Greenlee, Electrochemical recovery of phosphate from synthetic wastewater with enhanced salinity, Electrochimica Acta 426 (2022), 140848.
- [26] I. Wu, A. Teymouri, R. Park, L.F. Greenlee, A.M. Herring, Simultaneous electrochemical nutrient recovery and hydrogen generation from model wastewater using a sacrificial magnesium anode, Journal of The Electrochemical Society 166 (16) (2019) E576.
- [27] G.L. Song, A. Atrens, Corrosion Mechanisms of Magnesium Alloys, Advanced Engineering Materials 1 (1) (1999) 11–33.
- [28] G. Song, Recent Progress in Corrosion and Protection of Magnesium Alloys, Advanced Engineering Materials 7 (7) (2005) 563–586.
- [29] G. Song, A. Atrens, D. St John, X. Wu, J. Nairn, The anodic dissolution of magnesium in chloride and sulphate solutions, Corrosion science 39 (10–11) (1997) 1981–2004.
- [30] J. Huang, G.-L. Song, Y. Zhu, D. Zheng, Z. Wang, The anodically polarized Mg surface products and accelerated hydrogen evolution, Journal of Magnesium and Alloys (2021)
- [31] A. Clerici, S. Furfari, Challenges for green hydrogen development, 2021 AEIT International Annual Conference (AEIT), IEEE (2021) 1–6.
- [32] R. Sultana, L. Kékedy-Nagy, R. Daneshpour, L.F. Greenlee. Electrochemical Recovery of Phosphate from Synthetic Wastewater: Effects of Salinity, Ph, and Anode Potential, Ph, and Anode Potential.

- [33] L. Kékedy-Nagy, L. English, Z. Anari, M. Abolhassani, B.G. Pollet, J. Popp, L. F. Greenlee, Electrochemical nutrient removal from natural wastewater sources and its impact on water quality, Water Research 210 (118001) (2022) 1–13.
- [34] Y. Cai, Z. Han, X. Lin, J. Du, Z. Lei, Z. Ye, J. Zhu, Mechanisms of releasing magnesium ions from a magnesium anode in an electrolysis reactor with struvite precipitation, Journal of Environmental Chemical Engineering 10 (1) (2022), 106661.
- [35] J.D. Doyle, K. Oldring, J. Churchley, C. Price, S.A. Parsons, Chemical control of struvite precipitation, Journal of Environmental Engineering 129 (5) (2003) 419–426.
- [36] F. Foroughi, L. Kékedy-Nagy, M.H. Islam, J.J. Lamb, L.F. Greenlee, B.G. Pollet, The use of ultrasound for the electrochemical synthesis of magnesium ammonium phosphate hexahydrate (Struvite), ECS Transactions 92 (10) (2019) 47.
- [37] L. Zhou, D. Liu, S. Li, X. Yin, C. Zhang, X. Li, C. Zhang, W. Zhang, X. Cao, J. Wang, Z.L. Wang, Effective removing of hexavalent chromium from wasted water by triboelectric nanogenerator driven self-powered electrochemical system Why pulsed DC is better than continuous DC? Nano Energy 64 (2019), 103915.
- [38] E. Keshmirizadeh, S. Yousefi, M.K. Rofouei, An investigation on the new operational parameter effective in Cr (VI) removal efficiency: A study on electrocoagulation by alternating pulse current, J Hazard Mater 190 (1–3) (2011) 110, 124
- [39] Z.-H. Yang, H.-Y. Xu, G.-M. Zeng, Y.-L. Luo, X. Yang, J. Huang, L.-K. Wang, P.-P. Song, The behavior of dissolution/passivation and the transformation of passive films during electrocoagulation: Influences of initial pH, Cr (VI) concentration, and alternating pulsed current, Electrochimica Acta 153 (2015) 149–158.
- [40] T. Liu, J. Wang, X. Yang, M. Gong, A review of pulse electrolysis for efficient energy conversion and chemical production, Journal of Energy, Chemistry 59 (2021) 69–82
- [41] F. Rocha, Q. de Radiguès, G. Thunis, J. Proost, Pulsed water electrolysis: A review, Electrochimica Acta 377 (2021), 138052.
- [42] N. Shimizu, S. Hotta, T. Sekiya, O. Oda, A novel method of hydrogen generation by water electrolysis using an ultra-short-pulse power supply, Journal of applied electrochemistry 36 (4) (2006) 419–423.
- [43] N. Demir, M.F. Kaya, M.S. Albawabiji, Effect of pulse potential on alkaline water electrolysis performance, international journal of hydrogen energy 43 (36) (2018) 17013–17020.
- [44] A.H. Shaaban, Water electrolysis and pulsed direct current, Journal of the Electrochemical Society 140 (10) (1993) 2863.
- [45] I. Vincent, B. Choi, M. Nakoji, M. Ishizuka, K. Tsutsumi, A. Tsutsumi, Pulsed current water splitting electrochemical cycle for hydrogen production, International Journal of Hydrogen Energy 43 (22) (2018) 10240–10248.
- [46] W. Zhan, Y. Du, J. Lan, R. Lei, R. Li, D. Du, T.C. Zhang, Electrochemical degradation of indigo carmine by low voltage pulse electrolysis, Journal of Molecular Liquids 348 (2022), 118006.
- [47] D.T. Chin, Mass Transfer and Current-Potential Relation in Pulse Electrolysis, Journal of the Electrochemical Society 130 (8) (1983) 1657.
- [48] J. Shu, R. Liu, Z. Liu, J. Du, C. Tao, Manganese recovery and ammonia nitrogen removal from simulation wastewater by pulse electrolysis, Separation and purification technology 168 (2016) 107–113.
- [49] A. Kasach, D. Kharitonov, S. Radchenko, I. Zharskii, I. Kurilo, Effect of parameters of pulse electrolysis on electrodeposition of copper–tin alloy from sulfate electrolyte, Russian Journal of Electrochemistry 56 (9) (2020) 744–753.
- [50] R.R. Adžić, K.I. Popov, M.A. Pamić, Acceleration of electrocatalytic reactions by pulsation of potential: Oxidation of formic acid on Pt and Pt/Pbads electrodes, Electrochimica Acta 23 (11) (1978) 1191–1196.
- [51] L. Kékedy-Nagy, M. Abolhassani, R. Sultana, Z. Anari, K.R. Brye, B.G. Pollet, L. F. Greenlee, The effect of anode degradation on energy demand and production efficiency of electrochemically precipitated struvite, Journal of Applied Electrochemistry 52 (2) (2022) 205–215.
- [52] L. Martínez, M. Ramón, M. Cámara, M. Castilla, Batch and column adsorption of herbicide fluroxypyr on different types of Removal of Organics From Aqueous Solution 529 activated carbons from water with varied egrees of hardness and alkalinity, Water Res. 44 (2010) 879–885.

- [53] G. Song, A. Atrens, D. Stjohn, J. Nairn, Y. Li, The electrochemical corrosion of pure magnesium in 1 N NaCl, Corrosion Science 39 (5) (1997) 855–875.
- [54] Z. Shi, M. Liu, A. Atrens, Measurement of the corrosion rate of magnesium alloys using Tafel extrapolation, Corrosion science 52 (2) (2010) 579–588.
- [55] M. Esmaily, J. Svensson, S. Fajardo, N. Birbilis, G. Frankel, S. Virtanen, R. Arrabal, S. Thomas, L. Johansson, Fundamentals and advances in magnesium alloy corrosion, Progress in Materials Science 89 (2017) 92–193.
- [56] L. Kékedy-Nagy, M. Abolhassani, L.F. Greenlee, B.G. Pollet, An Electrochemical Study of Ammonium Dihydrogen Phosphate on Mg and Mg Alloy Electrodes, Electrocatalysis 12 (3) (2021) 251–263.
- [57] M. Santamaria, F. Di Quarto, S. Zanna, P. Marcus, Initial surface film on magnesium metal: A characterization by X-ray photoelectron spectroscopy (XPS) and photocurrent spectroscopy (PCS), Electrochimica Acta 53 (3) (2007) 1314-1324.
- [58] L. Kékedy-Nagy, A. Teymouri, A.M. Herring, L.F. Greenlee, Electrochemical removal and recovery of phosphorus as struvite in an acidic environment using pure magnesium vs. the AZ31 magnesium alloy as the anode, Chemical Engineering Journal 380 (2020) 1–7.
- [59] S.A. Ryder, Methods for comparing frequency response analysis measurements, Conference Record of the the, IEEE International Symposium on Electrical Insulation (Cat. No. 02CH37316), IEEE 2002 (2002) 187–190.
- [60] D.J. Kruk, M. Elektorowicz, J.A. Oleszkiewicz, Struvite precipitation and phosphorus removal using magnesium sacrificial anode, Chemosphere 101 (2014) 28–33.
- [61] L. Kékedy-Nagy, M. Abolhassani, S.I. Perez Bakovic, Z. Anari, J.P. Moore Ii, B. G. Pollet, L.F. Greenlee, Electroless Production of Fertilizer (Struvite) and Hydrogen from Synthetic Agricultural Wastewaters, Journal of the American Chemical Society 142 (44) (2020) 18844–18858.
- [62] D.H. Alsem, O.N. Pierron, E.A. Stach, C.L. Muhlstein, R.O. Ritchie, Mechanisms for fatigue of micron-scale silicon structural films, Advanced Engineering Materials 9 (1–2) (2007) 15–30.
- [63] J.R. Buchanan, C.R. Mote, R.B. Robinson, Thermodynamics of Struvite Formation, Transactions of the ASAE 37 (2) (1994) 617–621.
- [64] L. Kékedy-Nagy, L. English, Z. Anari, M. Abolhassani, B.G. Pollet, J. Popp, L. F. Greenlee, Electrochemical Nutrient Removal from Natural Wastewater Sources and its Impact on Water Quality, Water Research 210 (2022), 118001.
- [65] C.-C. Wang, X.-D. Hao, G.-S. Guo, M. Van Loosdrecht, Formation of pure struvite at neutral pH by electrochemical deposition, Chemical Engineering Journal 159 (1–3) (2010) 280–283.
- [66] S. Graeser, W. Postl, H.-P. Bojar, P. Berlepsch, T. Armbruster, T. Raber, K. Ettinger, F. Walter, Struvite-(K), KMgPO4· 6H2O, the potassium equivalent of struvite-a new mineral, European Journal of Mineralogy 20 (4) (2008) 629–633.
- [67] A. Krężel, W. Bal, A formula for correlating pKa values determined in D2O and H2O, Journal of Inorganic Biochemistry 98 (1) (2004) 161–166.
- [68] V.S. Stoll, J.S. Blanchard, [4] Buffers: Principles and practice, Methods in enzymology, Elsevier (1990) 24–38.
- [69] J. Yan, G. Springsteen, S. Deeter, B. Wang, The relationship among pKa, pH, and binding constants in the interactions between boronic acids and diols—it is not as simple as it appears, Tetrahedron 60 (49) (2004) 11205–11209.
- [70] H. Zöllig, C. Fritzsche, E. Morgenroth, K.M. Udert, Direct electrochemical oxidation of ammonia on graphite as a treatment option for stored source-separated urine, Water research 69 (2015) 284–294.
- [71] R. Bashar, K. Gungor, K. Karthikeyan, P. Barak, Cost effectiveness of phosphorus removal processes in municipal wastewater treatment, Chemosphere 197 (2018) 280–290.
- [72] T. Tunçal, F. İşgenç, A. Pala, Importance of EBPR efficiency on energy demand of full-scale wastewater treatment plants, Desalination and Water Treatment 22 (1–3) (2010) 292–298.
- [73] G. Bertanza, L. Menoni, G.U. Capoferri, R. Pedrazzani, Promoting biological phosphorus removal in a full scale pre-denitrification wastewater treatment plant, Journal of environmental management 254 (2020), 109803.